

# 7

## Nonparallel Flow: Instabilities of a Cylindrical Vortex

The cylindrical (or columnar) vortex is the simplest example of a non-parallel shear flow, and is a useful model for tornados and other geophysical vortices. Here we'll examine two classes of vortex instabilities: (1) **barotropic** instabilities are closely analogous to the instabilities of a parallel shear flow, while (2) **axisymmetric** instabilities resemble convection, but with the centrifugal force playing the role of gravity.

Consider a cylindrical coordinate system with **radial**, **azimuthal**, and **axial** coordinates  $r$ ,  $\theta$ , and  $z$  (Figure 7.1) and corresponding velocities  $u = dr/dt$ ,  $v = r d\theta/dt$ , and  $w = dz/dt$ . In geophysical applications, the axial direction usually coincides with the vertical.

Assuming inviscid, homogeneous flow, the equations are

$$\frac{1}{r} \frac{\partial}{\partial r} r u + \frac{1}{r} \frac{\partial v}{\partial \theta} + \frac{\partial w}{\partial z} = 0. \quad (7.1)$$

$$\frac{Du}{Dt} = \frac{v^2}{r} - \frac{\partial \pi}{\partial r} \quad (7.2)$$

$$\frac{Dv}{Dt} = -\frac{uv}{r} - \frac{1}{r} \frac{\partial \pi}{\partial \theta} \quad (7.3)$$

$$\frac{Dw}{Dt} = \frac{\partial \pi}{\partial z}, \quad (7.4)$$

where the material derivative is

$$\frac{D}{Dt} = \frac{\partial}{\partial t} + u \frac{\partial}{\partial r} + \frac{v}{r} \frac{\partial}{\partial \theta} + w \frac{\partial}{\partial z}, \quad (7.5)$$

[e.g., Smyth (2017), appendix I; Kundu et al. (2016), appendix B.6].

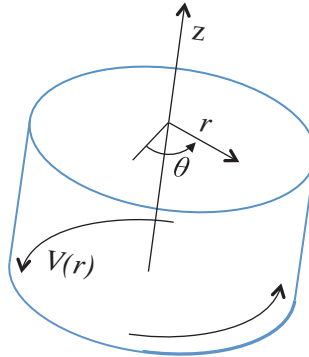


Figure 7.1 Axisymmetric (circular) vortex with cylindrical coordinates.

### 7.1 Cyclostrophic Equilibrium

We now seek an equilibrium state in which the flow is purely azimuthal:  $u = 0$ ,  $w = 0$ ,  $v = V(r)$ . This flow geometry is nondivergent, i.e., (7.1) is satisfied automatically. The momentum equations (7.2–7.4) become

$$\begin{aligned}\frac{V^2}{r} &= \frac{\partial \Pi}{\partial r} \\ \frac{\partial \Pi}{\partial \theta} &= 0 \\ \frac{\partial \Pi}{\partial z} &= 0.\end{aligned}$$

The pressure field can vary only in  $r$ , and is related to the azimuthal velocity by

$$\frac{d}{dr} \Pi(r) = \frac{V(r)^2}{r}. \quad (7.6)$$

This balance between the pressure gradient and the centrifugal force is called **cyclostrophic equilibrium**.

It is also useful to define the **angular velocity**:

$$\Omega(r) = \frac{V}{r},$$

the **axial vorticity**

$$Q(r) = \frac{1}{r} \frac{d}{dr} (rV),$$

and the **streamfunction**  $\Psi(r)$  such that

$$V(r) = -\frac{d\Psi}{dr}.$$

## 7.2 The Perturbation Equations

Now imagine a small perturbation to cyclostrophic equilibrium:

$$u = \epsilon u' ; \quad v = V(r) + \epsilon v' ; \quad w = \epsilon w' ; \quad \pi = \Pi(r) + \epsilon \pi'.$$

Substituting into (7.1–7.4) and linearizing, we obtain at  $O(\epsilon)$ :

$$\frac{1}{r} \frac{\partial}{\partial r} r u' + \frac{1}{r} \frac{\partial v'}{\partial \theta} + \frac{\partial w'}{\partial z} = 0. \quad (7.7)$$

$$\left[ \frac{\partial}{\partial t} + \Omega \frac{\partial}{\partial \theta} \right] u' = 2\Omega v' - \frac{\partial \pi'}{\partial r} \quad (7.8)$$

$$\left[ \frac{\partial}{\partial t} + \Omega \frac{\partial}{\partial \theta} \right] v' = -Q u' - \frac{1}{r} \frac{\partial \pi'}{\partial \theta} \quad (7.9)$$

$$\left[ \frac{\partial}{\partial t} + \Omega \frac{\partial}{\partial \theta} \right] w' = -\frac{\partial \pi'}{\partial z}. \quad (7.10)$$

**Exercise:** Fill in the algebra.

Since the coefficients of the linearized equations depend on  $r$ , we seek a normal mode solution with the  $r$ -dependence undetermined:

$$u' = \hat{u}(r) e^{\sigma t} e^{i(\ell\theta + mz)},$$

where  $\ell$  is an integer and only the real part is physically relevant. Substituting into the linearized equations (7.7–7.10) gives

$$\frac{1}{r} \frac{d}{dr} (r \hat{u}) + \frac{i\ell}{r} \hat{v} + i m \hat{w} = 0. \quad (7.11)$$

$$(\sigma + i\ell\Omega) \hat{u} = 2\Omega \hat{v} - \frac{d\hat{\pi}}{dr} \quad (7.12)$$

$$(\sigma + i\ell\Omega) \hat{v} = -Q \hat{u} - \frac{i\ell}{r} \hat{\pi} \quad (7.13)$$

$$(\sigma + i\ell\Omega) \hat{w} = -i m \hat{\pi}. \quad (7.14)$$

Two classes of perturbation are important and relatively easy to deal with.

- A **barotropic** perturbation has  $m = 0$ , i.e., no dependence on  $z$ . The first-mode barotropic instability has  $\ell = 1$  (Figure 7.2a), and shifts the entire vortex horizontally. Higher-order barotropic modes ( $\ell = 2, 3, \dots$ , Figure 7.2b,c, Figure 7.3) leave the vortex in place but distort its circular shape in increasingly ornate ways.
- The second important class of disturbances is the **axisymmetric modes**, also called **centrifugal instability**. These have  $\ell = 0$ , and hence no dependence on  $\theta$ , but  $m \neq 0$  (Figure 7.4a).

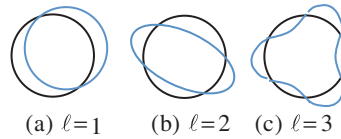


Figure 7.2 Barotropic perturbations of a circular vortex, seen in plan view. In all cases  $m = 0$ .

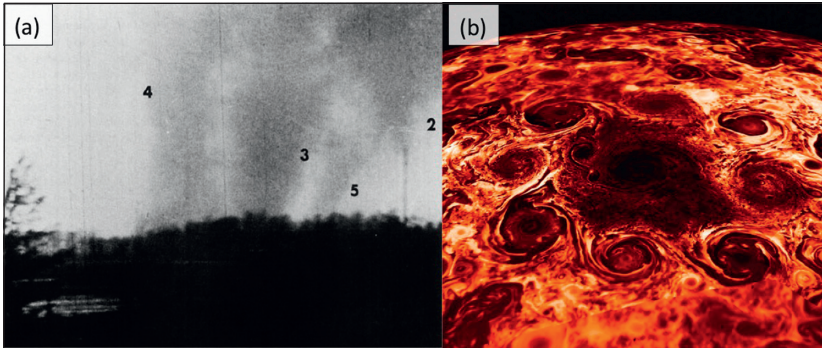


Figure 7.3 (a) Secondary vortices in a tornado suggestive of barotropic instability. Photo by W. Hubbard, WISH Indianapolis, from Snow (1978). (b) Instability with  $\ell = 8$  surrounding Jupiter's north polar vortex (courtesy NASA). Structures appear to be barotropic, extending as deep as 3000 km (Adriani et al., 2018; Kaspi et al., 2018).

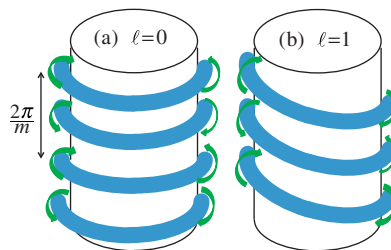


Figure 7.4 (a) Axisymmetric perturbation of a circular vortex. The mode takes the form of counter-rotating secondary vortices. (b) General, normal mode perturbation. In this case  $\ell = 1$ .

In each of these special cases there is a (relatively) easy way to collapse (7.11–7.14) into a single equation.

### 7.3 Barotropic Modes ( $m = 0$ )

For barotropic modes (Figures 7.2 and 7.3), the trick is to recognize that the perturbation flow is two-dimensional and nondivergent, and can therefore be represented by a streamfunction. We define  $\hat{\psi}$  such that

$$\hat{u} = \frac{\iota\ell}{r}\hat{\psi}; \quad \hat{v} = -\frac{d\hat{\psi}}{dr}.$$

Note that, with  $m = 0$ , (7.11) is satisfied exactly, and (7.14) gives  $\hat{w} = 0$ . Remaining are two equations for the two unknowns  $\hat{\psi}$  and  $\hat{\pi}$ . These combine to form

$$(\sigma + \iota\ell\Omega) \left[ \frac{d}{dr} \left( r \frac{d\hat{\psi}}{dr} \right) - \frac{\ell^2}{r} \hat{\psi} \right] = \iota\ell \frac{dQ}{dr} \hat{\psi}. \quad (7.15)$$

**Exercise:** Show this.

**Exercise:** Compare (7.15) with the Rayleigh equation (3.18). Identify and interpret the differences in each term.

### 7.3.1 Boundary Conditions for Barotropic Modes

- An impermeable boundary can be placed at any radius, say  $r = r_1$ . Impermeability requires that the radial velocity be zero at that boundary, i.e.,  $\hat{u} = 0$ , and assuming  $\ell \neq 0$ ,

$$\hat{\psi}(r_1) = 0.$$

- If the inner boundary is to be placed at  $r = 0$ , then we need an approximate solution for (7.15) that becomes exact as  $r \rightarrow 0$ . Suppose that  $\hat{\psi}$  is proportional to  $r^\alpha$ . Substituting into (7.15) and multiplying through by  $r^{1-\alpha}$ , we get

$$(\sigma + \iota\ell\Omega)(\alpha^2 - \ell^2) = \iota\ell r \frac{dQ}{dr} \hat{\psi}. \quad (7.16)$$

The background profiles  $\Omega(r)$  and  $Q(r)$  are not yet specified, but as long as  $dQ/dr$  is finite, the right-hand side goes to zero as  $r \rightarrow 0$ , and therefore as long as  $\sigma - \iota\ell\Omega \neq 0$ ,  $\alpha^2 - \ell^2 = 0$ . We choose the solution that is bounded as  $r \rightarrow 0$  and end up with

$$\hat{\psi} \propto r^\ell, \quad \text{or} \quad \hat{\psi}(0) = 0.$$

In numerical calculations it is not a problem to have the inner boundary at  $r = 0$ , even though  $r$  appears in the denominator of (7.15). This is because  $r_0 = 0$  is a ghost point, so nothing is ever actually evaluated there.

- If the outer boundary is at infinity, we can again assume that  $\hat{\psi} \propto r^\alpha$ , resulting again in (7.16). If we now assume that  $dQ/dr$  decays to zero faster than  $1/r$  as  $r \rightarrow \infty$ , then the right-hand side goes to zero, and if  $\sigma - \iota\ell\Omega \neq 0$  we again have  $\alpha = \pm\ell$ . The bounded solution is now  $\hat{\psi} \propto r^{-\ell}$ , and the boundary condition becomes

$$\lim_{r \rightarrow \infty} \hat{\psi}(r) = 0. \quad (7.17)$$

- In numerical calculations, we cannot actually place the outer boundary at infinity, so we place it at some large but finite radius (hopefully where  $dQ/dr$  has decreased almost to zero) and apply the asymptotic condition

$$\frac{d\hat{\psi}}{dr} = -\ell\hat{\psi}.$$

The perturbation equation (7.15) can then be reduced to a generalized eigenvalue problem using derivative matrices as in the case of parallel flows.

The matrix solution of (7.15) is analogous to the case of parallel shear flow. We first replace the derivatives with derivative matrices incorporating the appropriate boundary conditions. We then arrange the equation as an eigenvalue equation and find the eigenvalues and eigenvectors numerically.

**Admonition:** It may be tempting to define a first-derivative matrix  $\mathbf{D}^{(1)}$ , then use it twice to form the second-derivative. Don't do this – it effectively replaces the grid spacing  $\Delta$  by  $2\Delta$ , degrading the accuracy of the results. In (7.15), the first term in the brackets should be computed in the expanded form

$$\mathbf{D}^{(1)} + r \cdot \mathbf{D}^{(2)},$$

rather than the simpler but less accurate

$$\mathbf{D}^{(1)}r \cdot \mathbf{D}^{(1)}.$$

### 7.3.2 Stability Theorem for Barotropic Modes

We rewrite (7.15) as

$$\frac{d}{dr} \left( r \frac{d\hat{\psi}}{dr} \right) - \frac{\ell^2}{r} \hat{\psi} = \frac{\imath\ell\hat{\psi}}{\sigma + \imath\ell\Omega} \frac{dQ}{dr}, \quad (7.18)$$

then apply the operator  $\int_{r_1}^{r_2} \hat{\psi}^* dr$ . The radii  $r_1$  and  $r_2$  are the boundaries of the domain. The inner boundary radius may be  $r_1 = 0$ , and the outer may be  $r_2 = \infty$ .

The first term on the left gives

$$\int_{r_1}^{r_2} \hat{\psi}^* \frac{d}{dr} \left( r \frac{d\hat{\psi}}{dr} \right) dr = \hat{\psi}^* r \frac{d\hat{\psi}}{dr} \Big|_{r_1}^{r_2} - \int_{r_1}^{r_2} r \left| \frac{d\hat{\psi}}{dr} \right|^2 dr.$$

Using the boundary conditions derived in the previous subsection, the first term vanishes, leaving

$$\int_{r_1}^{r_2} \hat{\psi}^* \frac{d}{dr} \left( r \frac{d\hat{\psi}}{dr} \right) dr = - \int_{r_1}^{r_2} r \left| \frac{d\hat{\psi}}{dr} \right|^2 dr.$$

The second term on the left of (7.18) is just

$$\int_{r_1}^{r_2} \frac{\ell^2}{r} |\hat{\psi}|^2 dr.$$

Note that both of the above integrals are real. Applying the integral operator to the right-hand side and taking the imaginary part, we have

$$0 = \Im \int_{r_1}^{r_2} \frac{\iota \ell |\hat{\psi}|^2}{\sigma + \iota \ell \Omega} \frac{dQ}{dr} dr.$$

Multiplying and dividing the integrand by the complex conjugate  $\sigma^* - \iota \ell \Omega$  to isolate the imaginary part gives

$$0 = \ell \sigma_r \int_{r_1}^{r_2} \frac{|\hat{\psi}|^2}{|\sigma + \iota \ell \Omega|^2} \frac{dQ}{dr} dr.$$

For a growing (or decaying) mode,  $\sigma_r \neq 0$ , and therefore the integral must vanish, i.e.,  $dQ/dr$  must change sign at least once in  $r_1 < r < r_2$ .

**Theorem** *Given an inviscid, homogeneous, circular vortex, a necessary condition for barotropic instability is that the vorticity gradient  $dQ/dr$  change sign somewhere in the domain  $r_1 < r < r_2$ .*

Note the similarity between this and the inflection point theorem for parallel shear flows (section 3.11.1 or 3.15). As we will see later in this chapter, barotropic vortex instabilities and parallel shear flow instabilities have many properties in common. For these instabilities, it is not entirely wrong to think of the vortex as a parallel shear flow bent to form a circle. However, the curvature also introduces an important new effect: the centrifugal force. This effect is understood most simply in the context of axisymmetric modes, which we investigate next.

**Exercise:** Derive a Fjørtoft-type condition for barotropic vortex instabilities.

#### 7.4 Axisymmetric Modes ( $\ell = 0$ )

In the axisymmetric case  $\ell = 0$ , (7.11–7.14) can be combined into a single equation for the radial velocity perturbation  $\hat{u}$ :

$$\sigma^2 \left\{ \frac{d}{dr} \left[ \frac{1}{r} \frac{d}{dr} (r\hat{u}) \right] - m^2 \hat{u} \right\} = \Phi m^2 \hat{u}, \quad (7.19)$$

where

$$\Phi(r) = 2\Omega Q$$

is called the **Rayleigh discriminant**.

### 7.4.1 Boundary Conditions for Axisymmetric Modes

- If an impermeable boundary is placed at some  $r_1$ , then the radial velocity must vanish there, i.e., the boundary condition is just  $\hat{u}(r_1) = 0$ .
- Now suppose there is no inner boundary, so we need a virtual boundary condition at  $r = 0$ . Assume that, for  $r$  near zero,  $\hat{u}$  is proportional to  $r^\alpha$ . Substituting into (7.19) and multiplying through by  $r^{2-\alpha}$ , we obtain

$$\sigma^2\{\alpha^2 - 1 - m^2r^2\} = m^2r^2\Phi.$$

Assuming that  $\Phi$  remains finite, the right-hand side must vanish as  $r \rightarrow 0$ . Therefore, for nonzero  $\sigma$ , the quantity in braces must vanish as  $r \rightarrow 0$ , hence  $\alpha = \pm 1$ . To keep the solution bounded, we choose  $\alpha = 1$ , i.e.,  $\hat{u} \propto r$ . The boundary condition at  $r = 0$  is therefore

$$\hat{u}(0) = 0.$$

- If there is no outer boundary, we employ an asymptotic boundary condition. We will assume that the vortex is *isolated*, meaning that if you go far enough away, the vortex motion vanishes. More specifically,  $\Phi \rightarrow 0$  as  $r \rightarrow \infty$ . In that case, for sufficiently large  $r$ , (7.19) becomes

$$\frac{d}{dr} \left[ \frac{1}{r} \frac{d}{dr} (r\hat{u}) \right] - m^2\hat{u} = 0$$

This is the *modified Bessel equation* (Spiegel, 1968), and its bounded solution is the first-order modified Bessel function:

$$\hat{u} = K_1(mr).$$

As  $r \rightarrow \infty$ ,  $K_1$  can be approximated using Stirling's formula

$$K_1(mr) \approx \frac{e^{-mr}}{\sqrt{2\pi mr}}; \quad \text{for } mr \gg 1.$$

Therefore,  $\hat{u} \rightarrow 0$  in the limit  $r \rightarrow \infty$ .

- An asymptotic condition is also available for use in numerical calculations where the domain must be finite. Taking the logarithmic derivative of the Stirling approximation to  $K_1$ ,

$$\frac{1}{\hat{u}} \frac{d\hat{u}}{dr} = \frac{d}{dr} (\ln \hat{u}) = \frac{d}{dr} \left[ -mr - \frac{1}{2} \ln(2\pi mr) \right] = -m - \frac{1}{2r}.$$

So if the computation domain ends at  $r = R$ , the asymptotic boundary condition is

$$\frac{d\hat{u}}{dr} = - \left( m + \frac{1}{2R} \right) \hat{u}.$$

**7.4.2 Stability Theorem for Axisymmetric Modes**

We now apply the integral operator  $\int_{r_1}^{r_2} r \hat{u}^* dr$  to (7.19). Here,  $r_1$  and  $r_2$  are the boundaries of the domain. The inner boundary radius may be  $r_1 = 0$ , and the outer may be  $r_2 = \infty$ . We'll apply this operator individually to the two terms on the left-hand side and the single term on the right. The first term on the left, omitting the factor  $\sigma^2$  for now, gives

$$\begin{aligned} \int_{r_1}^{r_2} r \hat{u}^* \frac{d}{dr} \left[ \frac{1}{r} \frac{d}{dr} (r \hat{u}) \right] dr &= \hat{u}^* \frac{d}{dr} (r \hat{u}) \Big|_{r_1}^{r_2} - \int_{r_1}^{r_2} \frac{d}{dr} (r \hat{u}^*) \frac{1}{r} \frac{d}{dr} (r \hat{u}) dr \\ &= - \int_{r_1}^{r_2} \frac{1}{r} \left| \frac{d}{dr} (r \hat{u}) \right|^2 dr. \end{aligned}$$

Here, the boundary conditions derived in the previous subsection have been used. The second term (setting aside the factor  $-\sigma^2 m^2$ ) is

$$\int_{r_1}^{r_2} r \hat{u}^* \hat{u} dr = \int_{r_1}^{r_2} r |\hat{u}|^2 dr.$$

Finally, the right-hand side (omitting  $m^2$ ) is

$$\int_{r_1}^{r_2} r \Phi |\hat{u}|^2 dr.$$

Combining these results and restoring the various constants, we have

$$\sigma^2 \left\{ \int_{r_1}^{r_2} \frac{1}{r} \left| \frac{d}{dr} (r \hat{u}) \right|^2 dr + m^2 \int_{r_1}^{r_2} r |\hat{u}|^2 dr \right\} = -m^2 \int_{r_1}^{r_2} r \Phi |\hat{u}|^2 dr$$

or, with some rearranging

$$\sigma^2 \int_{r_1}^{r_2} \frac{1}{r} \left| \frac{d}{dr} (r \hat{u}) \right|^2 dr = -m^2 \int_{r_1}^{r_2} r |\hat{u}|^2 (\sigma^2 + \Phi) dr. \tag{7.20}$$

For  $\sigma^2 > 0$  the integral on the right must be negative, and therefore  $\sigma^2 + \Phi$  must be negative for some  $r$ . Therefore the minimum value of  $\Phi(r)$  must be less than  $-\sigma^2$ , or

$$\sigma < \sqrt{-\min_z(\Phi)}. \tag{7.21}$$

Instability is possible provided that  $\min_z(\Phi) < 0$ . This class of unstable modes is called **centrifugal instability**.

**Theorem** *Given an inviscid, homogeneous, circular vortex, a necessary condition for centrifugal instability is that the Rayleigh discriminant  $\Phi(r) = 2\Omega(r)Q(r)$  be negative for some  $r$ . Moreover, (7.21) gives an upper bound on the growth rate.*

**Centrifugal instability is closely analogous to convection.** To see this, note the similarity between (7.19) and (2.29), the equation for convective instability in an inviscid, nondiffusive fluid with arbitrary stratification  $B_z(z)$ . The Rayleigh discriminant  $\Phi(r)$  is the analog of stratification. In the convective case, if  $B_z < 0$ , the fluid possesses gravitational potential energy that can be converted to kinetic energy. Here, a variant of potential energy due to the centrifugal force is available for conversion to kinetic energy wherever  $\Phi < 0$ . Also compare the growth rate bound (7.21) for centrifugal instability with the upper bound on the convective growth rate, (2.34). This analogy is discussed in greater detail later in section 7.8.

### 7.5 Analytical Example: the Rankine Vortex

The Rankine vortex has uniform vorticity  $2\Omega_0$  inside a radius  $R$  and zero vorticity outside (Figure 7.5, black curves). It is a useful model for localized vortices such as tornadoes. The vorticity gradient is given by

$$\frac{dQ}{dr} = -2\Omega_0\delta(r - R) \quad (7.22)$$

There is no radius at which the vorticity gradient changes sign, so there is no possibility of barotropic instability. How about centrifugal instability? The azimuthal velocity profile is

$$V(r) = \begin{cases} \Omega_0 r, & \text{for } r \leq R \\ \Omega_0 \frac{R^2}{r}, & \text{for } r \geq R \end{cases} \Rightarrow \Phi(r) = \begin{cases} 4\Omega_0^2, & \text{for } r \leq R \\ 0, & \text{for } r \geq R \end{cases} \quad (7.23)$$

With no negative values of  $\Phi$ , there can be no centrifugal instability.

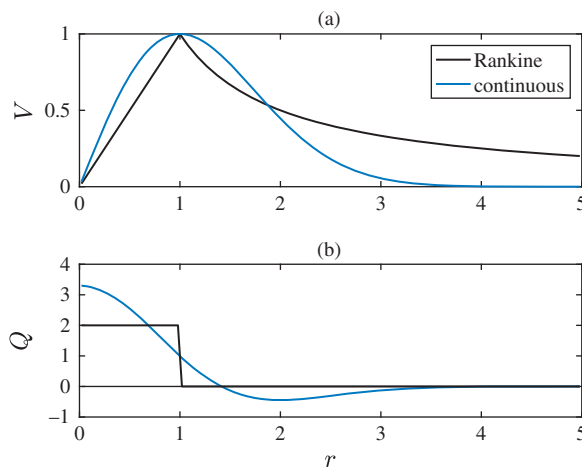


Figure 7.5 Profiles of velocity (a) and vorticity (b) for the Rankine vortex (7.23) with  $\Omega_0 = R = 1$  and the continuous vortex (7.29).

*Barotropic Waves on a Rankine Vortex*

Although the Rankine vortex is stable, its barotropic wave modes are of interest. (Finding the wave modes of the axisymmetric case is left as an exercise.) We will find it convenient to define the complex angular velocity of the perturbation,

$$\omega = \frac{\iota\sigma}{\ell},$$

and rewrite (7.15) as

$$\frac{d}{dr} \left( r \frac{d\hat{\psi}}{dr} \right) - \frac{\ell^2}{r} \hat{\psi} = \frac{dQ/dr}{\Omega - \omega} \hat{\psi}. \tag{7.24}$$

Except at  $r = R$ , the right-hand side of (7.24) is zero. As was noted in section 7.3.1, solutions then have the form  $\hat{\psi}(r) \propto r^{\pm\ell}$ . Applying the boundary conditions  $\hat{\psi} \rightarrow 0$  as  $r \rightarrow 0$  and  $\infty$  and requiring continuity across  $r = R$  leads to

$$\hat{\psi}(r) = A \begin{cases} (r/R)^\ell & , r < R \\ (r/R)^{-\ell} & , r > R \end{cases} \tag{7.25}$$

with  $A$  an arbitrary constant.

The dispersion relation is obtained as in the analysis of both convection at an interface (section 2.2.4) and the instability of a piecewise-linear shear layer (section 3.3). A jump condition is found by integrating (7.24) across the delta function in (7.22):

$$\lim_{\epsilon \rightarrow 0} \int_{R-\epsilon}^{R+\epsilon} \frac{d}{dr} \left( r \frac{d\hat{\psi}}{dr} \right) dr - \lim_{\epsilon \rightarrow 0} \int_{R-\epsilon}^{R+\epsilon} \frac{\ell^2}{r} \hat{\psi} dr = \lim_{\epsilon \rightarrow 0} \int_{R-\epsilon}^{R+\epsilon} \frac{-2\Omega_0 \delta(r - R)}{\Omega - \omega} \hat{\psi} dr. \tag{7.26}$$

The first integral is trivial, and the second goes to zero as its range of integration vanishes because its integrand is finite. The right-hand side simplifies by using properties of the delta function (Figure 2.5), leaving us with the jump condition:

$$\left[ \left[ r \frac{d\hat{\psi}}{dr} \right] \right]_R = \frac{-2\Omega_0}{\Omega_0 - \omega} \hat{\psi}(R). \tag{7.27}$$

After substituting  $\left[ \left[ r \frac{d\hat{\psi}}{dr} \right] \right]_R = -2A\ell$  and  $\hat{\psi}(R) = A$  from (7.25), we arrive at the dispersion relation

$$\omega = \Omega_0 + \frac{\Delta Q_0}{2\ell} = \Omega_0 \left( 1 - \frac{1}{\ell} \right). \tag{7.28}$$

This describes a vorticity wave being advected around the core of the vortex with angular velocity  $\Omega_0$  while propagating with an intrinsic phase speed  $-\Delta Q_0/2\ell = \Omega_0/\ell$ . Note the similarity to the dispersion relation of the vorticity waves from section 3.13.1. The wave propagates upstream relative to the vortex. The fundamental

mode  $\ell = 1$ , with intrinsic phase speed  $-\Omega_0$ , is stationary. Modes with higher wavenumbers ( $\ell > 1$ ) are unable to keep up with the advective speed and therefore precess in the same sense as the vortex.

More complex profiles can support multiple wave modes. Like instability in an inviscid shear layer, barotropic instability of a circular vortex can result from the resonant interaction of these waves, as is described below in section 7.7.

## 7.6 Numerical Example: a Continuous Vortex

We now consider a vortex with a continuous azimuthal velocity profile, nondimensionalized so that both the maximum flow and the radius of maximum flow are unity (Figure 7.5, blue curves):

$$V = r e^{-\frac{1}{2}(r^2-1)}; \quad Q = (2 - r^2) e^{-\frac{1}{2}(r^2-1)}. \quad (7.29)$$

### 7.6.1 Barotropic Modes

Because the vorticity gradient changes sign at  $r = 2$ , barotropic instability is possible (section 7.3.2). In fact, the barotropic mode with  $\ell = 2$  is unstable as shown in Figure 7.6a. The streamfunction eigenfunction has maximum amplitude just inside  $r = 2$ , the inflectional radius, and the phase shifts rapidly near this radius. The sign of the phase shift is such that phase lines of the radial velocity tilt against the vorticity. This is the circular analog of the instability of a parallel shear flow (Chapter 3).

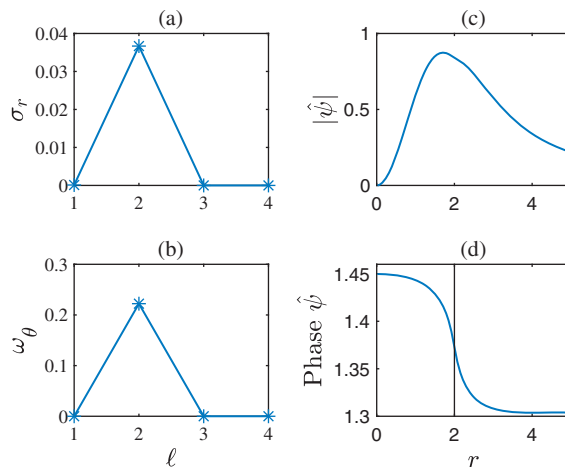


Figure 7.6 Growth rate (a) and frequency (b) versus azimuthal wavenumber for barotropic modes of (7.29). Amplitude (c) and phase (d) profiles for the fastest-growing barotropic mode. Vertical line shows the radius of minimum vorticity (cf. Figure 7.5).

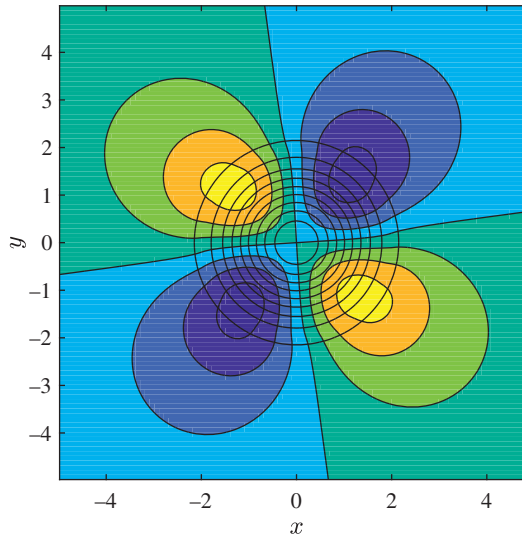


Figure 7.7 Streamfunction for the fastest-growing barotropic mode of (7.29). Circles are streamlines of the background flow.

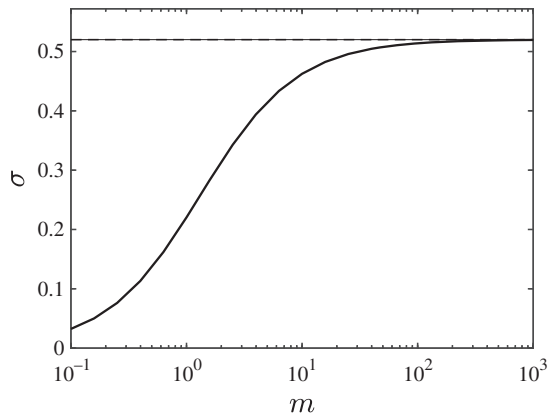


Figure 7.8 Growth rate versus axial wavenumber for axisymmetric modes. Dashed line shows Rayleigh's upper bound  $\sqrt{-\Phi_{min}}$ .

The velocity perturbation causes the vortex to bulge inward and outward as in Figure 7.2b. The mode is not stationary; it precesses around the vortex with azimuthal velocity about one-fifth that of the maximum flow speed (Figure 7.6b).

### 7.6.2 Axisymmetric Modes

The Rayleigh discriminant  $2\Omega Q$  is negative for  $r > \sqrt{2}$  (where  $Q < 0$ , Figure 7.5b). We therefore suspect axisymmetric instability, and that suspicion is confirmed in the numerical results (Figure 7.8). There is no preferred axial scale:

the growth rate increases monotonically with increasing axial wavenumber. This is broadband instability, as we found previously for convective instability of an inviscid fluid (section 2.2). As  $m \rightarrow \infty$ , the growth rate approaches the maximum value  $\sqrt{-\Phi_{min}}$ .

The radial velocity is greatest near  $r = \sqrt{3}$ , where  $\Phi$  is most negative. As  $m$  is increased, the eigenfunction becomes more tightly concentrated near that radius. The result is a stack of counter-rotating vortices surrounding the background vortex, as sketched in Figure 7.4a.

**Exercise:** Derive a perturbation kinetic energy budget analogous to (3.56) based on (7.7–7.10).

### 7.7 Wave Interactions in Barotropic Vortices

Recall from Chapter 3 that instabilities of a parallel shear flow may be interpreted as resonant wave interactions. Here we develop an equivalent view for barotropic modes of a circular vortex. Consider a background profile  $V(r)$  that has a concentric, piecewise-uniform vorticity distribution. The vorticity gradient is composed of a series of delta functions:

$$\frac{dQ}{dr} = \sum_i \Delta Q_i \delta(r - R_i), \quad (7.30)$$

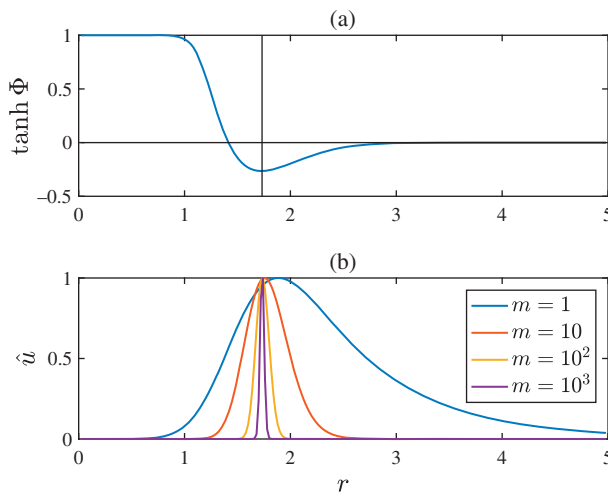


Figure 7.9 (a) Profile of the Rayleigh discriminant  $\Phi = 2\Omega Q$  of (7.29), scaled using the tanh function to make the minimum visible. The vertical line indicates  $r = \sqrt{3}$ , where  $\Phi$  is a minimum. (b) Eigenfunction of the radial velocity for various  $m$ .

where  $\Delta Q_i$  is the jump in vorticity across each vorticity interface, located at  $r = R_i$ . The advantage of choosing this type of profile (equivalent to the piecewise-linear representation of a parallel shear flow) is that it replaces the governing equation with the simpler form

$$\frac{d}{dr} \left( r \frac{d\hat{\psi}}{dr} \right) - \frac{\ell^2}{r} \hat{\psi} = 0. \quad (7.31)$$

This form applies between the interfaces, and has a solution that was already found in our look at the Rankine vortex in section 7.5. Writing the solution (7.25) in a slightly more general form, for a single interface at  $r = R_i$  we have

$$\hat{\psi}(r) = A_i G(r, R_i) \quad \text{where} \quad G(r, R_i) = \begin{cases} (r/R_i)^\ell & , r < R_i \\ (r/R_i)^{-\ell} & , r > R_i \end{cases}. \quad (7.32)$$

The function  $G(r, R_i)$  can be thought of as an ‘‘influence function’’<sup>1</sup> describing the decay of the interfacial disturbance from its peak at  $r = R_i$  (Figure 7.10). Note that, as in the case of the shear layer, the amplitude of  $G$  decays more rapidly with increased wavenumber ( $\ell$ , in this case), so that longer waves are ‘‘felt’’ over a greater distance. The solution for  $N$  interfaces is

$$\hat{\psi}(r) = \sum_{i=1}^N A_i G(r, R_i). \quad (7.33)$$

The remaining step is to connect this solution, which applies *between* the interfaces, with jump conditions that apply *at* the interfaces. The required jump condition is given above in (7.27). Substituting (7.33), we have

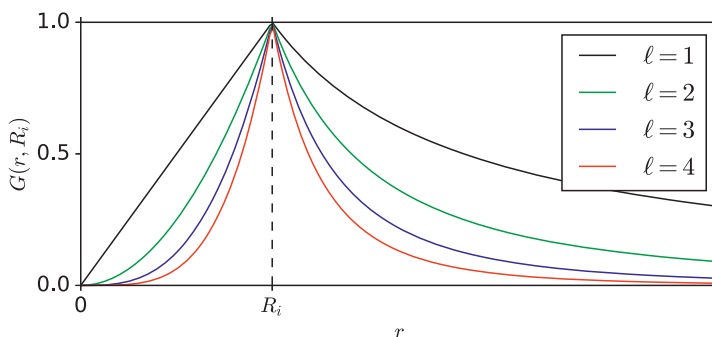


Figure 7.10 Structure of the influence function,  $G(r, R_i)$ , in a barotropic vortex arising from a vorticity interface located at  $r = R_i$  (dashed line).

<sup>1</sup> More precisely, this is the Green’s function for the linear differential operator in (7.31). The use of Green’s functions is a more general approach to solving this type of problem.

$$-2\ell A_i = \frac{\Delta Q_i}{2\ell(\Omega_i - \omega)} \sum_{j=1}^N A_j G(R_i, R_j). \quad (7.34)$$

With a little rearranging, we can write this as

$$\omega A_i = \sum_{j=1}^N \left\{ \Omega_i I_{ij} + \frac{\Delta Q_i}{2\ell} G_{ij} \right\} A_j, \quad (7.35)$$

where  $I$  is the  $N \times N$  identity matrix and  $\mathbf{G}$  is the influence matrix, defined by  $G_{ij} = G(R_i, R_j)$ . The quantity enclosed in braces is an  $N \times N$  matrix, each of whose  $N$  eigenvalues is the angular velocity  $\omega$  for one of the  $N$  eigenmodes. If  $\omega$  has a positive imaginary part, the mode is unstable. The corresponding eigenvector contains the coefficients  $A_i$  that define the radial dependence of the amplitude.

### *Example: a General Two-Interface Vortex*

We now look at a general example of a barotropic vortex that consists of two vorticity interfaces, located at  $r = R_1$  and  $r = R_2$  and having magnitudes  $\Delta Q_1$  and  $\Delta Q_2$ . The influence matrix is

$$\begin{bmatrix} 0 & \delta^\ell \\ \delta^\ell & 0 \end{bmatrix}$$

where  $\delta = R_1/R_2$ .

According to (7.35), the phase velocities are given by the eigenvalue equation

$$\begin{bmatrix} \Omega_1 + \frac{\Delta Q_1}{2\ell} & \frac{\Delta Q_1}{2\ell} \delta^\ell \\ \frac{\Delta Q_2}{2\ell} \delta^\ell & \Omega_2 + \frac{\Delta Q_2}{2\ell} \end{bmatrix} \begin{bmatrix} A_1 \\ A_2 \end{bmatrix} = \omega \begin{bmatrix} A_1 \\ A_2 \end{bmatrix}. \quad (7.36)$$

In the special case of a single interface at  $r = R_1$ , with vorticity change  $\Delta Q_1 = -2\Omega_1$ , we set  $\delta = \Omega_2 = \Delta Q_2 = 0$ . Our eigenvalue problem (7.36) then simplifies to

$$\omega_1 = \Omega_1 + \frac{\Delta Q_1}{2\ell} \quad (7.37)$$

which is equivalent to (7.28). Alternatively, the single interface could be located at  $R_2$ , in which case

$$\omega_2 = \Omega_2 + \frac{\Delta Q_2}{2\ell}. \quad (7.38)$$

In terms of those frequencies, the eigenvalues of (7.36) are

$$\omega = \frac{\omega_1 + \omega_2}{2} \pm \left[ \left( \frac{\omega_1 - \omega_2}{2} \right)^2 + \Delta Q_1 \Delta Q_2 \frac{\delta^{2\ell}}{4\ell^2} \right]^{1/2}. \quad (7.39)$$

In order to have instability the vorticity jumps must have opposite sign:  $\Delta Q_1 \Delta Q_2 < 0$ . Compare this result with the theorem proven in section 7.3.2.

Note also that we recover the undisturbed phase speeds if the strength of the interaction between the two waves, described by the factor  $\delta^{2\ell}$ , goes to zero. This is equivalent to increasing the distance between the two interfaces indefinitely so that the velocity perturbations decay to zero and the waves become uncoupled.

## 7.8 Mechanisms of Centrifugal and Convective Instabilities

As we noted in section (7.4.2), the stability equations (7.19) for centrifugal instability and (2.29) for convection are very similar. In fact, the only differences are due to the cylindrical geometry of the former. Here we will describe the mechanisms of the two instabilities in terms that will highlight the parallels between the two.

In the convectively unstable background state sketched in Figure 7.11, dense fluid overlies light fluid.

- (i) If a downward flow  $w'$  is initiated at some point (thick blue arrow), the density at that point will increase in time.
- (ii) The resulting change in the buoyancy force,  $F'$ , is directed downward (thin blue arrow), and hence accelerates the downward flow.
- (iii) Consistent with mass conservation, this downward motion is accompanied by upward motion at some other location. There, the reverse process happens: the buoyancy force is perturbed so as to accelerate the upward motion (red arrows).

In the case of centrifugal instability, the background azimuthal velocity at some radius decreases with distance from the vortex center. On the right-hand side of the vortex sketched in Figure 7.12, the background flow is directed into the page.

- (i) A radially outward flow is initiated at some point (thick red arrow). It carries with it a positive perturbation in azimuthal velocity, and thus an increase in the centrifugal force (thin red arrow).

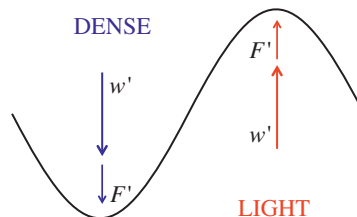


Figure 7.11 Perturbations involved in the convective instability of a statically unstable buoyancy distribution.

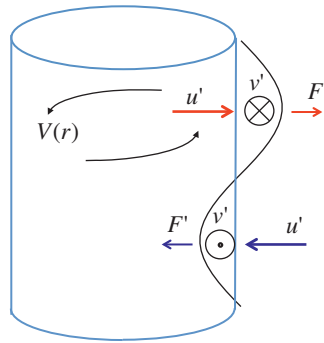


Figure 7.12 Perturbations involved in the centrifugal instability of a circular vortex. The radial motion  $u$  advects the background azimuthal velocity to create a perturbation,  $F$ , in the centrifugal force.

- (ii) The disturbance in the force is directed outward, and hence accelerates the outward flow.
- (iii) The outward motion is accompanied by inward motion at some other location. There, the reverse process happens (blue arrows): the centrifugal force is perturbed so as to accelerate the inward motion.

**Exercise:** Examine the perturbation equations for each of these instabilities and identify the terms that correspond to the three-part processes described above.

### 7.8.1 Universality of the Fastest-Growing Mode

When inspecting Figure 7.8, you may have noticed that the growth rate actually reaches the upper bound  $\sqrt{-\min_r(\Phi)}$  in the limit  $m \rightarrow \infty$ . There is nothing special about the profile (7.29); in fact, it appears that this is a general property of both centrifugal and convective instabilities in an inviscid fluid. Specifically, the upper bound we have derived for the growth rate is actually reached in the limit of large wavenumber ( $\tilde{k}$  for convection,  $m$  for centrifugal instability), regardless of the details of the profile  $B_z$  (or  $\Phi$ ), provided only that it includes at least one negative local minimum as required by the stability theorem. An example for convective instability is found in homework problem 16 (Appendix A).

To see why this may be so, consider the convective example illustrated in Figure (7.13), which shows a negative local minimum of  $B_z$ . If we zoom in to a small enough scale, the variability of  $B_z$  becomes negligible, and the solution of the perturbation equation (2.29) should be similar to the solution for constant  $B_z$  (section 2.2.2). In the limit of large wavenumber, the motions are locally vertical, and the growth rate is equal to the upper bound,  $\sqrt{-B_z}$ . Therefore, the fastest-growing mode has growth rate  $\sqrt{-\min_z(B_z)}$  regardless of the detailed shape of  $B(z)$ . In project B.7, you will have the opportunity to examine this result rigorously.

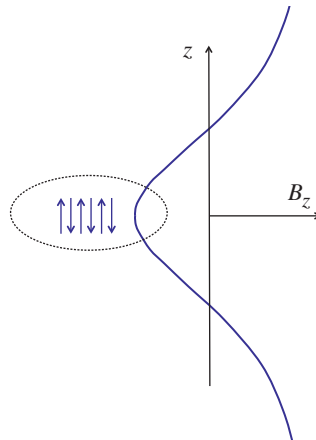


Figure 7.13 Convective instability near a negative local minimum in a generic stratification profile  $B_z(z)$ .

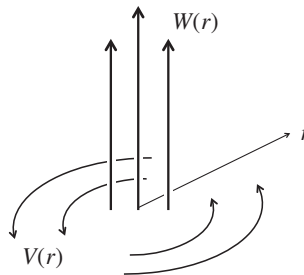


Figure 7.14 Cylindrical vortex with axial flow.

Note that:

- The result holds only in the inviscid limit. In a viscous fluid, motions on sufficiently small scales are damped. As a result, there is a preferred wavenumber having growth rate smaller than the inviscid upper bound.
- This class of instabilities (convective, centrifugal, and others that we'll encounter in Chapter 8) bypasses the usual turbulent energy cascade. Rather than beginning a sequential process in which motions excite successively smaller motions until viscous dissipation takes over, the instability transfers energy directly to the smallest-scale motions allowed by viscosity.

## 7.9 Swirling Flows

Vortical flows in nature are frequently accompanied by flow in the axial (typically vertical) direction. Tornadoes and hurricanes, for example, are powered largely by rising air in their centers. Conversely, deep convection in both atmosphere and ocean usually involves some degree of rotation. Figure 7.14 shows a simple model

in which nothing varies in the axial or azimuthal directions, but the radially varying azimuthal background flow  $V(r)$  is accompanied by an axial component  $W(r)$ .

To keep the math simple we will assume that the disturbance, like the background flow, is axisymmetric:

$$\begin{aligned} u' &= \epsilon u'(r, z, t), & v &= V(r) + \epsilon v'(r, z, t), & w &= W(r) + \epsilon w'(r, z, t), \\ \pi &= \Pi(r) + \epsilon \pi'(r, z, t). \end{aligned} \quad (7.40)$$

Substituting into (7.1–7.5), we find that the cyclostrophic equilibrium condition (7.6) is unchanged. The equations for axisymmetric perturbations can be simplified using the normal mode solution

$$u'(r, z, t) = \hat{u}(r)e^{im(z-ct)},$$

where only the real part is retained and similar forms apply for  $v'$ ,  $w'$ , and  $\pi'$ .

The linearized continuity equation is

$$\frac{1}{r} \frac{d}{dr}(r\hat{u}) + im\hat{w} = 0. \quad (7.41)$$

We can therefore write the radial and axial perturbations in terms of a streamfunction:

$$\hat{u} = -im\hat{\psi}(r); \quad \hat{w} = -\frac{1}{r} \frac{d}{dr} r\hat{\psi}(r).$$

Note that we do not assume that the flow is two-dimensional. The radial and axial velocities can be described by a streamfunction because the azimuthal perturbation, while nonzero, is independent of  $\theta$ , and therefore does not enter into (7.41).

After the usual manipulations, which the student is encouraged to check, we arrive at

$$\frac{d}{dr} \left[ \frac{1}{r} \frac{d}{dr} \left( r \frac{d\hat{\psi}}{dr} \right) \right] + \left[ \frac{\Phi}{(W-c)^2} - \frac{Z}{W-c} + m^2 \right] \hat{\psi} = 0, \quad (7.42)$$

where

$$Z = \frac{1}{r} \frac{d}{dr} r \frac{dW}{dr}.$$

Now, here is something amazing. Ready?

Take a close look at (4.18), the Taylor-Goldstein equation for stratified shear flow, and compare it term by term with (7.42). The two are practically isomorphic, the only difference being that the form of the  $r$ -derivatives is modified due to the cylindrical geometry. In place of  $B_z$  we have the Rayleigh discriminant  $\Phi$ , showing again that  $\Phi$  represents a gradient in the centrifugal force having the same effect as the buoyancy gradient. The place of  $U_{zz}$  is taken by  $Z$ , the radial gradient of the vorticity due to the axial parallel shear flow  $W(r)$ , and the axial wavenumber  $m$  takes the place of  $k$ .

Basically everything we learned about inviscid parallel shear flows in Chapters 3 and 4 can be turned on its side, bent around into a circle, and applied to swirling flows.

- If the axial flow contains an inflection point, it can produce shear instability just as  $U(z)$  does, the only difference being that the resulting vortices are circular. Smoke rings are an example.
- If  $\Phi > 0$ , the centrifugal force tends to oppose the instability just as gravity does with Kelvin-Helmholtz instability when  $B_z > 0$ . In this case there is an analog to the Miles-Howard theorem:  $\Phi/(dW/dr)^2$ , the analog of the gradient Richardson number, must be  $< 1/4$  at some  $r$  for instability to be possible (Howard and Gupta, 1962).
- The axial phase velocity  $c$  must lie within a semicircle bounded by the maximum and minimum of  $W$  (cf. Howard's semicircle theorem).

### 7.10 Summary

A circular vortex exhibits two relatively simple instability types corresponding to barotropic ( $m = 0$ ) and axisymmetric ( $\ell = 0$ ) disturbances. The instabilities are related to shear and convective instabilities, respectively. Both the mechanisms of the instabilities and the general theorems that govern them follow precisely as in the previous discussions (Chapters 2 and 3).

### 7.11 Further Reading

See Terwey and Montgomery (2002) for a more detailed analysis of barotropic instabilities of the concentric, piecewise-uniform vorticity distribution. The original theory of swirling flow instabilities is in Howard and Gupta (1962).